Tailoring Fluorescence Brightness and Switching of Nanoparticles through Dye Organization in the Polymer Matrix

Andreas Reisch,[§*‡] *Kateryna Trofymchuk,*[§‡] *Anne Runser,*[§] *Guillaume Fleith,*[#] *Michel Rawiso,*[#] *and Andrey S. Klymchenko*[§*]

[§:] Laboratoire de Biophotonique et Pharmacologie, UMR CNRS 7213, Université de Strasbourg, 74 route du Rhin, 67401 Illkirch Cedex, France

E-mail: reisch@unistra.fr and andrey.klymchenko@unistra.fr

[#]: Institut Charles Sadron (CNRS-UdS), 23 rue du Loess, BP 84047, 67034 Strasbourg Cedex 2, France

[‡:] These authors have contributed equally to experiments and data analysis.

Keywords: Fluorescent nanoparticles, dye-loaded polymer nanoparticles, excitation energy transfer, blinking/switching/fluorescence intermittency, fluorescence imaging

Abstract:

Fluorescent nanoparticles (NPs) help to increase spatial and temporal resolution in bioimaging. Advanced microscopy techniques require very bright NPs that either exhibit stable emission for single-particle-tracking or complete on/off-switching (blinking) for superresolution imaging. Here, ultrabright dye-loaded polymer NPs with controlled switching properties are developed. To this aim the salt of a dye (rhodamine B octadecyl ester) with a hydrophobic counterion (fluorinated tetraphenyl borate) is encapsulated at very high concentrations up to 30 wt% in NPs made of poly(lactic-*co*-glycolic acid) (PLGA), poly(methyl methacrylate) (PMMA), and polycaprolactone (PCL) through nanoprecipitation. The obtained 35 nm NPs are nearly 100 times brighter than quantum dots. The nature of the polymer is found to define the collective behavior of the encapsulated dyes, so that NPs containing thousands of dyes exhibit either whole particle blinking, for PLGA, or stable emission, for PMMA and PCL. Fluorescence anisotropy measurements together with small angle X-ray scattering experiments suggest that in less hydrophobic PLGA, dyes tend to cluster, whereas in more hydrophobic PMMA and PCL, dyes are dispersed within the matrix, thus altering switching behavior of NPs. Experiments using a perylene-diimide derivative show a similar effect of the polymer nature. The resulting fluorescent nanoparticles are suitable for a wide range of imaging applications from tracking to superresolution imaging. The findings on organization of the load will have impact on development of materials for applications ranging from photovoltaics to drug delivery.

Introduction

Spatial organization of emitters plays a crucial role in the manipulation of photons inside materials. For example, the photonic properties of inorganic materials depend on the precise positioning of the constituent atoms or ions and the placement of defect sites, yielding such extraordinary materials as luminescent quantum dots,[1,2] photo-voltaic systems based on perovskites,[3,4] or upconverting nanoparticles.[5,6] Controlling periodicities at the nanometer scale leads to photonic crystals with their applications ranging from thin film optics over light transmission to optical computers.[7,8] Soft organic materials are often more eco-friendly and more appropriate for biological applications due to the absence of heavy metal compounds, their potential biodegradability, and the ease with which they can be interfaced with biological systems.[9] In such materials interactions with photons are often achieved *via* species that can absorb and/or emit light (chromophores / fluorophores / dyes), and their organization defines specific photonic properties of the materials as a whole. However, achieving an ordering at the molecular scale in soft organic materials is considerably more challenging. As the spatial organization of fluorophores plays a crucial role, e.g., in governing excitation energy transfer (EET) processes,[10] nature has nevertheless found ways: This is beautifully exemplified in the case of light-harvesting complexes, capable of channeling light energy over tens of nanometers to the photosynthetic centers due to a finely controlled positioning of the dyes by proteins.[11,12] Chemists did also gain a high level of control through precisely positioning the dyes in complex molecules, such as dendrimers[13,14] and artificial light-harvesting complexes,[15,16] or by designing molecules presenting aggregation-induced emission (AIE) behavior[17] or formation of optically active liquid crystalline phases.[18] However, this requires long and precise synthesis, which ultimately limits the number of fluorophores that can be integrated in these systems and their

large-scale production. In this respect, a more straightforward yet very promising platform for soft photonic materials is polymer matrices encapsulating chromophores.

A control of the properties at the nanometer level can be readily achieved in such materials by creating dye-loaded thin polymer films[19] or polymer nanoparticles.[9,20,21] Controlling the organization of the chromophores on a molecular to film/particle level is, however, much more challenging. In the case of dye-loaded polymer nanoparticles achieving such control is of particular importance in view of the recent interest they have attracted as bright fluorescent labels for bioimaging.[20,21] For these applications the first key parameter is the brightness of the used label, which ultimately defines the number of photons collected in a given amount of time.[22] Until recently the brightness of dye-loaded polymer NPs was strongly limited due to so-called aggregation-caused quenching of fluorophores at high dye loadings.[20,21] One possibility to overcome this limitation, is controlling the short-range ordering of the dyes, notably to avoid formation of non-emissive H-aggregates through pi-stacking.[23] This can be achieved, for example, through modification of the fluorophores with bulky side-groups[24–26] and/or by providing the dye with propeller-like topology to achieve AIE behavior.[17,20] Another approach, which was recently proposed by us, is the encapsulation of charged dyes with bulky hydrophobic counterions (*e.g.* F5-TPB, Figure 1) in polymer NPs.[27] The counterions are thought to act as spacers that prevent π-stacking of the encapsulated dyes into non-fluorescent aggregates. The counterion approach enabled preparation of 40 nm NPs based on poly(lactic-*co*-glycolic acid) (PLGA) NPs presenting 6 to 10 times higher brightness than corresponding quantum dots.[27,28] The second key parameter for bioimaging applications is the behavior of the particle emission over time. On the one hand, a continuous emission greatly facilitates tracking of the emitters. On the other hand, resolving emitters at distances below the diffraction limit, achieved using direct

stochastic optical reconstruction microscopy (dSTORM) [29,30] or photo-activated localization microscopy (PALM),[31] requires fluorescence intermittency due to blinking or photoactivation. In the case of quantum dots, blinking is an inherent property, but tuning and especially avoiding it was - and still is - a huge challenge.[32–34] Fluorescence intermittency in dye-loaded polymer NPs is even more challenging as it requires controlling the collective behavior of >100 encapsulated dyes. In the case of our PLGA particles loaded with R18/F5-TPB a collective on-off-switching of practically all the dyes in one particle leading to an unprecedented whole particle blinking occurred.[27] This phenomenon was attributed to ultra-fast excitation energy migration among practically all the dyes in one particle. Recently, we showed that the excitation energy in these systems can propagate over $>10^4$ dyes at the sub-picosecond time scale, so that a single energy acceptor could collect the energy from this large dye ensemble resulting in light-harvesting phenomena with antenna effects of >1000.[35] However, it remained unclear how to tune this collective behavior of dyes and thus the particle blinking.

In this paper, we describe our findings that the nature of the matrix polymer used to assemble dye-loaded nanoparticles through nanoprecipitation modulates the organization of the dye load and, thus, the optical properties of the nanomaterials. We thus investigated in detail the influence of the polymer on the fluorescence properties, when the NPs were loaded with increasing amounts of a dye salt, R18/F5-TPB, or a perylene diimide (PDI-1). Besides PLGA we chose two other readily available biocompatible polymers: poly(methyl methacrylate-*co*-methacrylic acid) (containing 1.5 % acid groups, noted PMMA here), and acid terminated polycaprolactone (PCL). The achieved control over dye organization yielded, on the one hand, high QYs at very high loading. On the other hand, we studied the collective behavior of the dyes within one NP and how these are linked to the organization of the dyes. The findings presented here were thus used

to create ultrabright fluorescent nanoparticles with controlled dye organization and thus fluorescence properties: Notably color, and blinking behavior - ranging from whole particle on-off switching to its complete absence - could be tailored in this way, which will enable applications ranging from single particle tracking to superresolution imaging.

Experimental section

Materials: Poly(D,L-lactide-*co*-glycolide) (PLGA, lactide 50 mole%, glycolide 50 mole%, acid terminated, M_n 24,000, PDI 1.7), polycaprolactone (α,ω-dihydroxy functional, M_n ~10,000, M_w ~14,000), poly(methyl methacrylate-*co*-methacrylic acid) (PMMAMA noted here as PMMA, 1,3 % methacrylic acid, M_n ~15,000, M_w ~34,000), *N*,*N*-Diisopropylethylamine (DIPEA, 99,5%), acetonitrile (anhydrous, 99.8%), rhodamine B octadecyl ester perchlorate (>98.0%), lithium tetrakis(pentafluorophenyl)borate ethyl etherate, were purchased from Sigma-Aldrich. Succinic anhydride was purchased from AlfaAesar. N,N′-Bis(1-heptyloctyl)-3,4,9,10-perylenebis-(dicarboximide) (PDI-1) was synthesized from 1-heptyloctylamine (Sigma-Aldrich) and perylene-3,4,9,10-tetracarboxylic dianhydride (Sigma-Aldrich) as was described previously.[36] Polycaprolactone with terminal COOH groups was synthesized from α,ω-dihydroxy functional polycaprolactone and succinic anhydride according to a procedure described previously.[28] R18/F5-TPB, the salt of Rhodamine B octadecyl ester with tetrakis(pentafluorophenyl)borate, was synthesized through dye exchange followed by purification through column chromatography as described previously.[27] Sodium phosphate monobasic (>99.0%, Sigma-Aldrich) and sodium phosphate dibasic dihydrate (>99.0%, Sigma-Aldrich) were used to prepare 20 mM phosphate buffer solutions at pH 7.4. MilliQ-water (Millipore) was used in all experiments. Qdot® 585 Streptavidin Conjugates and Fluospheres®

(carboxylate-modified microspheres, 0.02 μm, given lot size 0.028 μm, measured: DLS 33 nm, TEM 30 nm, nile red λ_{ex} 535 nm, λ_{em} 575nm), were purchased from Thermo-Fisher Scientific.

Preparation of NPs: Solutions of the polymers in acetonitrile (2 mg mL^{-1} for PLGA, 1 mg mL^{-1} for PMMA and PCL), containing different amounts of dye (from 0 to 30 wt% relative to the polymer) were added quickly and under stirring (shaking) using a micropipette to a 10-fold volume excess of 20 mM phosphate buffer at pH 7.4. PLGA and PMMA based nanoparticles were prepared at 21 °C, PCL nanoparticles were prepared at 27 °C. The particle solution was then quickly diluted five-fold with the same buffer.

Electron Microscopy: 5 μL of the particle solution were deposited onto carbon-coated copper-rhodium electron microscopy grids that were used either as obtained or following an air or amylamine glow-discharge. The grids were then treated for 1 min with a 2 % uranyl acetate solution for staining and observed with a Philips CM120 transmission electron microscope equipped with a LaB_6 filament and operating at 100 kV. Areas covered with NPs of interest were recorded at different magnifications on a Peltier cooled CCD camera (Model 794, Gatan, Pleasanton, CA). Image analysis was performed using the Fiji software.

Spectroscopy: Absorption and emission spectra were recorded on a Cary 400 Scan UV-visible spectrophotometer (Varian) and a FluoroMax-4 spectrofluorometer (Horiba Jobin Yvon) equipped with a thermostated cell compartment, respectively. For standard recording of fluorescence spectra, the excitation wavelength was set to 530 nm and emission was recorded from 540 to 700 nm for R18, and excitation at 485 nm and emission from 510 nm to 750 nm were used for PDI-1. *Steady-state anisotropy* was measured on a SLM 8000 spectrofluorometer (Aminco) in a T-configuration. Quantum yields were calculated using rhodamine 101 in ethanol (QY = 0.9) with an absorbance of 0.01 at 530 nm as a reference.[37]

Time-resolved Fluorescence: Measurements were performed with the time-correlated, single-photon counting technique using the excitation pulses at 480 nm provided by a pulse-picked frequency doubled Ti-sapphire laser (Tsunami, Spectra Physics) pumped by a Millenia X laser (Spectra Physics). The emission was collected through a polarizer set at the magic angle and an 8 nm band-pass monochromator (Jobin-Yvon H10) at 582 nm. The instrumental response function was recorded with a polished aluminium reflector, and its full-width at half-maximum was 40 ps. For lifetime measurements the decays were analyzed using the minimum entropy method. For time-resolved anisotropy measurements, the fluorescence decay curves were recorded at the vertical and horizontal positions of the excitation polarizer and with the emission polarizer set to the vertical position, and analyzed by the following equation:

$$r(t) = \frac{I_v(t) - G \cdot I_h(t)}{I_v(t) + 2 \cdot G \cdot I_h(t)} \qquad (1)$$

where I_v and I_h are the intensities collected at vertical and horizontal excitation polarizations, respectively, and G is the geometry factor at the emission wavelength, determined in independent experiments.

Fluorescence Microscopy: For single particle fluorescence microscopy measurements the NPs were immobilized on glass surfaces on which a polyethyleneimine (PEI) layer was initially adsorbed. The solutions of NPs were diluted to a particle concentration of about 6 pM with water. 400 µL of these solutions per cm^2 were then brought in contact with the PEI covered glass for 15 min, followed by extensive rinsing with MilliQ-water. The surfaces were left in MilliQ-water during microscopy. Quantum dots and Fluospheres were immobilized and imaged in the same way as the NPs.

Single particle measurements were performed in the TIRF (Total Internal Reflection Fluorescence) mode on a home-made wide-field setup based on an Olympus IX-71 microscope

with an oil immersion objective (NA = 1.49, 100x). A DPPS (Cobolt) continuous wave (CW) laser emitting at 532 nm was used for excitation at 0.5 or 5 $W.cm^{-2}$. The fluorescence signal was recorded with an EMCCD (ImagEM Hamamatsu) using an exposure of 30.5 ms per image frame. Single particle analysis was performed using the Fiji software as described previously[27,28] (see SI for details).

Small-Angle X-Ray Scattering (SAXS): Experiments were performed with a diffractometer developed by Molecular Metrology (Elexience, France) that uses a Rigaku Micromax 007HF generator with a copper rotating anode. The wavelength of the incident X-ray beam is $\lambda = 0.154$ nm. This diffractometer operates with a pinhole collimation of the X-ray beam focused by a multilayer optic designed by Osmic and a two-dimensional gas-filled multiwire detector. The sample–detector distance was set at $D = 0.7$ m, leading to a range of scattering vectors covered by the experiment $0.1 < q < 3.2$ nm^{-1}. The scattering vector q is defined by $q = (4\pi/\lambda) \times \sin(\theta/2)$, where λ is the wavelength of the incident beam and θ is the scattering angle. Cells of 1 mm thickness and calibrated Mica windows were used as sample holders. Measurements were performed at room temperature. Data were treated according to a standard procedure for isotropic SAXS as described in the Supporting Information, and the resulting scattering curves were then normalized using the Porod invariant Q in order to correct for differences in concentration and scattering length density, or more precisely contrast factor.

Results

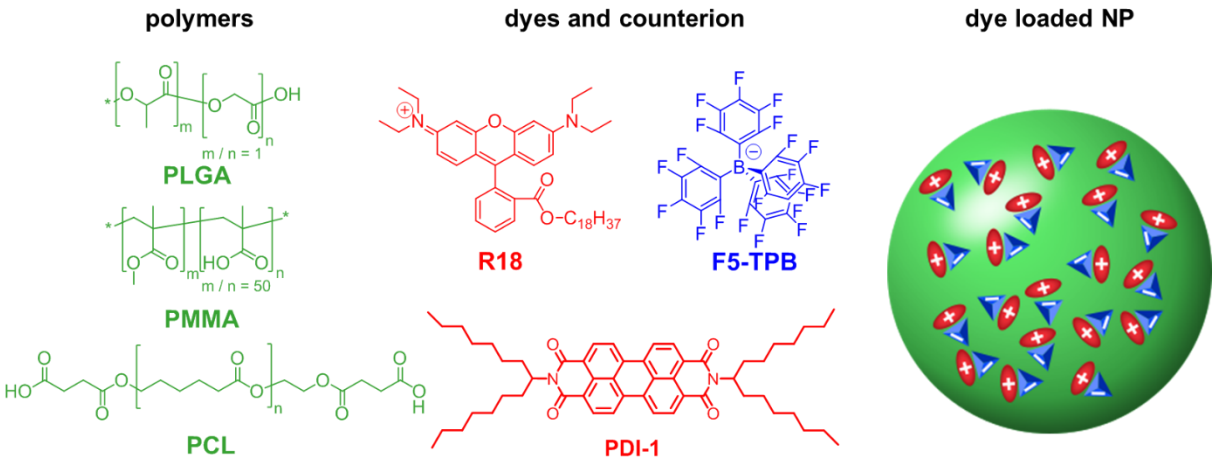

Figure 1. Dye-loaded nanoparticles: Structures of the polymers poly(lactic-*co*-glycolic acid) (PLGA), poly(methyl methacrylate-*co*-methacrylic acid) (noted PMMA here), and acid terminated polycaprolactone (PCL), of the dye rhodamine B octadecyl ester (R18) and its counterion tetrakis(pentafluorophenyl)borate (F5-TPB), and of the dye PDI-1 used in this study, and schematic representation of a dye-loaded polymer nanoparticle.

Size and Steady State Fluorescence

Dye-loaded NPs were obtained through nanoprecipitation of an acetonitrile solution of the polymer and the dye salt R18/F5-TPB (with varying dye salt concentration expressed here as wt% relative to the polymer) in aqueous phosphate buffer. The sizes of the obtained NPs increased slightly for all three polymers with increasing dye loading from around 26 nm for unloaded NPs to about 33 nm for 30 wt% loading according to transmission electron microscopy (TEM; Figure 2 a, b and Table 1, Supporting Information Figure S1, S2). Previous studies showed that encapsulation of the R18/F5-TPB dye-counterion pair was nearly quantitative in PLGA[27] and PMMA.[28] Therefore, we can estimate the mean number of dye molecules per NP (Table 1), which was of the order of 2200 to 2500 fluorophores per NP at the highest loadings.

For these series of NPs we then measured the steady state absorption and fluorescence properties (Figure 2, c-f). In the case of PLGA NPs, increasing dye loading led to a blue shift of the absorption maximum, a broadening of the absorbance spectra, and an increase in the relative contribution of the short-wavelength shoulder. There is notably a strong evolution of the spectrum when going from 0.2 to 1 wt% of dye loading. Such spectral changes are notably associated with the formation of H-type dimers or aggregates of dyes.[38] All these effects of dye loading were far less pronounced in the case of PMMA and especially PCL NPs, where the contribution of the short-wavelength shoulder was close to that for the free dye in solution. The emission maxima showed a slight red shift with increasing dye loading, together with a reduction in the width of the spectra, most pronounced for PLGA. The narrowing of emission band is in line with earlier observations on pure clusters of R18 with excess of F5-TPB counterions.[39] Though the quantum yields (QYs) decreased with increasing dye loading (Figure 2 c), they remained elevated even at high dye content in all three polymers (>20% in all cases for 10 wt%). For comparison, encapsulation of the same dye with the inorganic counterion perchlorate led to a QY of 2 % already at 5 wt% loading,[27] which demonstrates the efficiency of the use of the bulky fluorinated counterion F5-TPB in decreasing aggregation caused quenching. For a given dye loading the QYs increased in the following order PLGA < PCL < PMMA. For all polymers fluorescence lifetimes decreased with dye loading, in line with the QY decrease (SI Fig. S3 and Table S1). For PLGA NPs significant contributions of shorter lifetimes were observed, while the mean lifetime was above those for PMMA and PCL NPs. In view of the lower QYs for PLGA this hints to contributions of still faster decay components that could not be measured with our setup (< 30 ps).

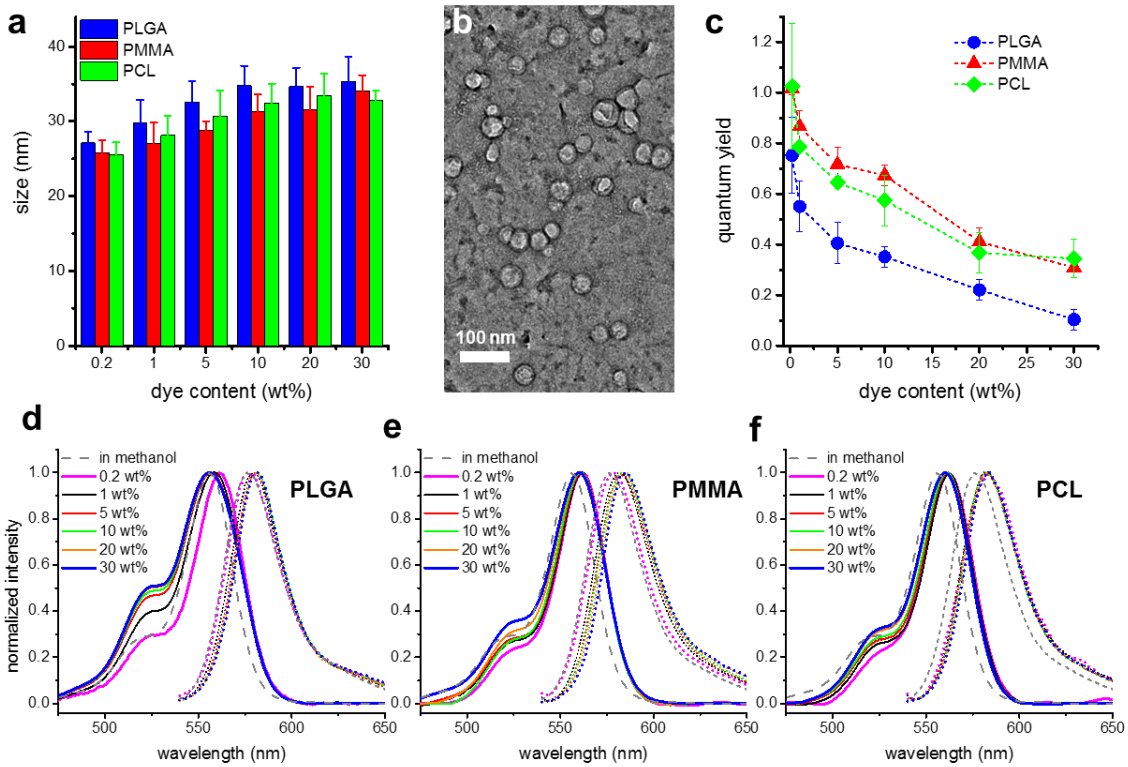

Figure 2. Size and steady state absorption/emission properties of NPs made from different polymers and loaded with different amounts of R18/F5-TPB: (a) Mean size of NPs as measured by transmission electron microscopy. Error bars correspond to s.e.m. (b) TEM image of PLGA NPs loaded with 5 wt% R18/F5-TPB. (c) Quantum yields of nanoparticles. QYs were determined relative to rhodamine 101 as standard (QY = 0.9) using an excitation at 530 nm. Given values are averages over at least 3 measurements. Normalized absorption (closed line) and emission spectra (dashed) of (d) PLGA, (e) PMMA, and (f) PCL NPs loaded with different amounts of R18/F5-TPB and comparison to the spectra of R18/F5-TPB in methanol (lowest and highest loading in bold). Emission spectra were recorded using an excitation at 530 nm.

Combining the measured QYs with the estimated number of fluorophores per NP and an extinction coefficient of 100 000 $M^{-1}cm^{-1}$ for the used rhodamine dye, the NP brightness could be calculated (Table 1, SI Table S3 for fluorescence cross section). The steady state brightness of these NPs increased continuously due to the increasing dye concentration and the high QYs, except for PLGA, where the brightness leveled off above 10 wt% loading. At the highest dye loadings studied here the values for PMMA and PCL NPs reached close to 10^8 $M^{-1}cm^{-1}$ corresponding to brightnesses nearly 1000 times higher than those of single fluorophores. PMMA and PCL NPs also showed a significantly higher photostability than PLGA NPs (SI Fig. S4).

Table 1. Size and fluorescence characteristics of NPs depending on dye loading and polymer.

dye loading		PLGA				PMMA				PCL			
wt%	mM	Size [nm][a]	N[b]	QY[c]	Brightness [$M^{-1}cm^{-1}$][d]	Size [nm]	N	QY	Brightness [$M^{-1}cm^{-1}$]	Size [nm]	N	QY	Brightness [$M^{-1}cm^{-1}$]
0.2	1.5	27	9	0.75	7.3×10^5	26	8	1.00	8.5×10^5	26	8	1.00	8.3×10^5
1	7	30	61	0.55	3.6×10^6	27	45	0.87	4.3×10^6	28	51	0.79	4.2×10^6
5	36	33	396	0.41	1.7×10^7	29	273	0.72	2.1×10^7	31	332	0.65	2.3×10^7
10	73	35	963	0.35	3.6×10^7	31	700	0.67	5.0×10^7	32	784	0.57	4.8×10^7
20	145	35	1906	0.22	4.5×10^7	32	1443	0.41	6.3×10^7	33	1716	0.37	6.7×10^7
30	218	35	3045	0.10	3.3×10^7	34	2724	0.31	8.9×10^7	33	2427	0.34	8.9×10^7

[a] NP diameters according to TEM measurements, for errors see Fig. 2 a; [b] estimated number of dyes per NP; [c] Quantum yields measured with Rhodamine 101 as reference, for errors see Fig. 2 c; [d] Calculated according to $B = \varepsilon \cdot QY$, with ε the extinction coefficient of the dye (100 000 M-1cm-1).

Single-Particle Fluorescence

The fluorescence of these three series of dye-loaded NPs was then studied on a single-particle level. Total internal reflection fluorescence (TIRF) microscopy of particles adsorbed on a surface was used to access single particle brightness and fluorescence transients. At an excitation power density of 0.5 W/cm^2 the single particle brightness increased initially strongly with dye loading, followed by a less strong increase at higher loadings (Figure 3). PMMA and PCL showed much steeper increases in brightness at loadings above 1 wt% compared to PLGA. At a tenfold higher excitation power density of 5 W/cm^2 the different NPs followed the same trends, but the brightness saturated at medium to high loadings (Figure 3 c). For example in the case of PMMA the brightness increased up to 10 wt% but then decreased upon further increase in dye-loading. A better idea of the NP brightness can be obtained by comparing them to external standards: under the same measurement conditions the brightest PLGA, PMMA, and PCL NPs were, respectively, *ca.* 2, 5, and 3 fold brighter than commercial Fluospheres®, and 45, 90, and 75 fold brighter than corresponding QDs. We also estimated the absolute brightness of our NPs using standardized parameters, such as the ratio of detected photons per second to the excitation power density (B, SI Table S2)[40] as well as fluorescence cross section (σ, Table S3).

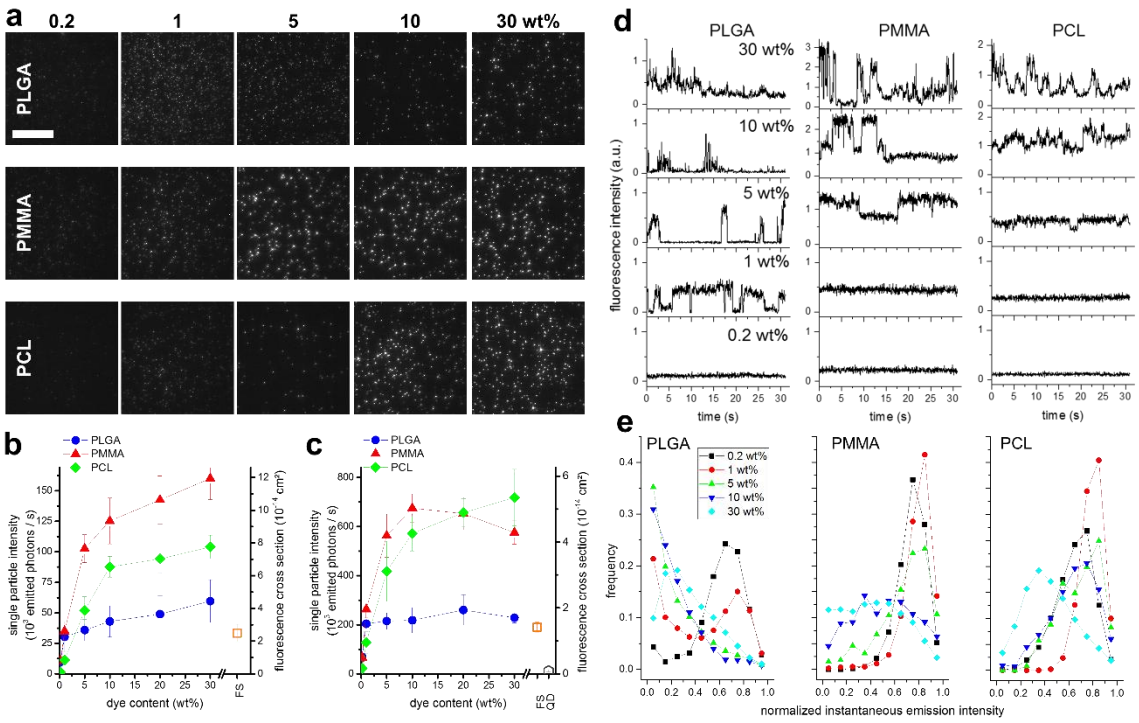

Figure 3. Single particle imaging of nanoparticles made from different polymers and loaded with different amounts of R18/F5-TPB. (a) Microscope images of NPs immobilized on a surface in TIRF mode using an illumination power density of 0.5 W/cm^2. Scale bar corresponds to 20 µm. (b, c) Mean brightness, expressed as emitted photons per second and fluorescence cross section, for at least 1000 particles as measured by TIRF microscopy using a 532 nm laser with an illumination power density of (b) 0.5 W/cm^2 and (c) 5 W/cm^2. FS: Fluospheres 535/575 0.028 µm, QD: Qdot streptavidin conjugates 585. Error bars give s.e.m. over three measurements. (d) Single particle intensity traces of NPs made from different polymers with different amounts of R18/F5-TPB. Given are representative transients as measured using TIRF microscopy using a 532 nm laser with an illumination power density of 0.5 W/cm^2. (e) Histograms of the normalized instantaneous emission intensities extracted from transients recorded under the same conditions (normalized relative to the maximum intensity). About 500 NPs per condition were analyzed.

A still more remarkable difference between the NPs made from different polymers appeared when the fluorescence signal of single NPs was recorded as a function of time (Figure 3 d and Supplementary videos). At very low dye loading all three types of NPs showed a nearly constant fluorescence. However, starting from 1 wt% of dye loading, virtually all PLGA NPs showed a practically complete whole particle blinking, in line with our previous report.[27] With increasing dye loading the duration of the on-state and the on-to-off-time ratio decreased (SI Figure S5). At very high dye loadings (starting from 20 wt%) the blinking was not complete anymore, and the PLGA NPs remained partially on.

For both, PMMA and PCL NPs, the behavior was very different: these NPs showed a constant fluorescence at 1 wt% dye loading. At 5 wt% loading the particles did not blink, but in many cases stepwise intensity modulations of less than 20 % of the particle intensity appeared. With increase in loading the amplitudes of the stepwise modulations increased and their durations decreased. At 30 wt% dye loading, finally, 50 % of the PMMA and 20 % of the PCL particles exhibited a practically complete on-off-blinking (off-state below 15% of the on-state brightness). Experiments on PMMA NPs of different sizes loaded with 30 wt % dye showed that the blinking amplitude also depends on NP size (SI Figure S6): 65 % of NPs of 24 nm (made from PMMA bearing sulfonate groups[28]) showed practically complete blinking, while this was only the case for less than 10 % of 60 nm NPs (made at 2 g/L of PMMA in buffer at pH 6.9).

In order to analyze the blinking behavior of a large number of NPs, we created histograms of the instantaneous single-particle fluorescence intensities (Figure 3 e, normalized to maximum NP intensity). At very low loading (0.2 wt%) all the particles are constantly in the on-state, resulting in a single clear maximum at around 0.8 (< 1 because of shot noise). At 1 wt% loading, a second maximum appeared for PLGA NPs at a value close to 0. The two maxima or peaks at 0.8 and 0

thus correspond to the on-and the off-state, respectively. The similar intensity of the two peaks (with the off-state peak being slightly higher) agrees well with the measured relative on-time of PLGA NPs with 1 wt% loading of 37% (SI Figure S5). Increasing the loading led to a relative decrease in the intensity of the peak of the on-state.

By contrast, in the cases of PMMA and especially PCL NPs the single peak at high relative emission intensity, corresponding to the on-state, is maintained for both small and medium loadings as these particles show stable on-state fluorescence. At the highest loadings the position of the peak shifted to lower values, corresponding to the appearance of partial blinking. Thus, at low and medium dye loading, blinking behavior was observed only for PLGA, while at high loading at least partial blinking was observed for all polymers. Especially in the case of PMMA NPs extremely large blinking amplitudes can be observed at high loading (up to 600 000 detected photons cm^2 W^{-1} s^{-1}). These can be >5000-fold higher than those typically encountered in single dyes (around 100 detected photons cm^2 W^{-1} s^{-1}),[40] and nearly 100-fold higher than those of semiconductor quantum dots,[34] although they are still smaller than the blinking amplitudes encountered in individual crystals of metal-organic perovskites of much larger size (up to 10 000 000 detected photons cm^2 W^{-1} s^{-1}).[41]

Fluorescence Anisotropy and Förster Resonance Energy Transfer

Excitation energy transfer inside the NPs was then studied to further understand the observed differences in the ensemble behavior of the encapsulated dyes.[42] As energy transfer between randomly oriented dyes leads to depolarization of the emitted light,[43,44] we measured steady-state and time-resolved fluorescence anisotropy of these NPs (Figure 4). The steady-state anisotropy decreased much faster with dye-loading for PLGA NPs than for PMMA and PCL NPs,

especially in the region up to 1 wt%. At this loading the anisotropy values were, respectively, 0.01, 0.04, and 0.06 for PLGA, PMMA, and PCL NPs.

Lifetime anisotropy measurements showed that at 1 wt% of dye loading, PLGA NPs experienced a very fast initial anisotropy decrease with a decay time of less than 20 ps, which is below the resolution of the instrument, followed by a plateau corresponding to a residual anisotropy of 0.011.[27] For PMMA and PCL NPs at the same dye loading, the decays are much slower and well described with stretched exponentials:

$$r(t) = r_0 \cdot \exp\left(-\left(\frac{t}{\tau_a}\right)^b\right) + r_\infty \qquad (2)$$

having decay times τ_a of, respectively, 180 and 300 ps and a stretching exponent b of 0.5, which is expected for randomly distributed fluorophores.[45–47] In these cases the residual anisotropy r_∞ was about 0.021 for PMMA and 0.025 for PCL, but this plateau value was only reached after about 4 ns (*versus* <100 ps for the PLGA NPs). At a dye loading of 5 wt% the decays were very fast for all 3 types of NPs, although for PMMA and PCL they were slower compared to PLGA. Already after less than 150 ps for PLGA and 200 ps for PMMA and PCL the anisotropy reached a plateau corresponding to a residual anisotropy close to zero in all three cases (about 0.001 ± 0.001).

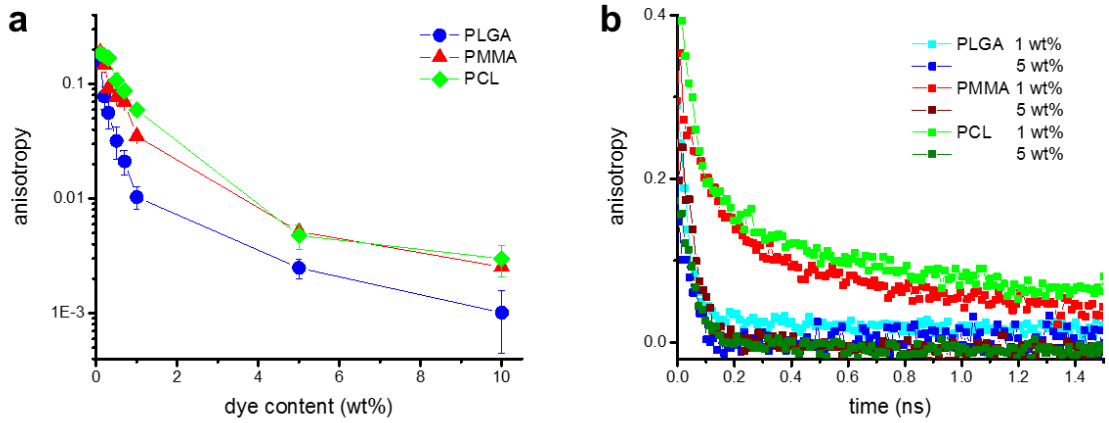

Figure 4. Fluorescence anisotropy of NPs. (a) Steady-state fluorescence anisotropy of nanoparticles made from different polymers and loaded with different amounts of R18/F5-TPB (λ_{ex} = 530 nm). Given values are averages over at least 3 measurements, error bars correspond to s.e.m. (b) Anisotropy decays of nanoparticles made from different polymers and loaded with 1 or 5 wt% of R18/F5-TPB.

In the cases of our dye-loaded NPs the dyes are thought to be immobilized in the polymer matrix, and the rotational correlation times of objects of the size of our NPs are of the order of hundreds of ns. In consequence, the decrease in the fluorescence emission anisotropy in these systems is expected to be mainly due to the transfer of excitation energy among fluorophores. Comparison of the different polymer NPs with respect to their steady-state and time-resolved anisotropy suggests that this energy transfer is the fastest in the case of PLGA particles, suggesting smaller inter-fluorophore distances in PLGA NPs compared to PMMA and PCL. The residual anisotropy obtained in these experiments can be used to estimate the mean number of fluorophores involved in energy transfer.[47–49] Here, we assume that (i) orientation of the dyes inside NPs is random and (ii) these dye emitters are energetically identical, in agreement with the almost negligible variation of the emission bandwidth at different dye loadings (Figure 2d-f).

The second assumption would mean that the dye-dye energy transfer is reversible. Then, in the system with finite number *N* of dyes coupled by fast energy transfer: $N = r_0/r_\infty$,[47] where r_0 is the fundamental anisotropy (0.37 for rhodamine[50]) and r_∞ is the residual anisotropy. At 1 wt% loading, the *N* values are about 35, 17, and 15, respectively for PLGA, PMMA, and PCL NPs. Remarkably, for PLGA NPs the value is close to the mean number of fluorophores per NP (see Table 1). At 5 wt% loading, the residual anisotropies were of the order of 0.001 for all three polymers, giving an *N* of 370, which suggests that hundreds of fluorophores are involved in energy transfer within a particle. We should note that the obtained *N* values are rough estimations of the upper limit to the number of randomly oriented fluorophores implicated in the reversible energy transfer. In cases, where the energy transfer becomes irreversible, the anisotropy can already drop to values of $r_0/25$ after a single transfer step.[48,49,51]

In order to have further insight in the energy transfer within the NPs, we then compared the experimental results with theoretical calculations. Förster theory allows estimating the expected anisotropy decay times for a given concentration of randomly distributed fluorophores according to[43]:

$$\tau_a = 0.0508 \frac{\tau_0}{R_0^6 C^2} \qquad (3)$$

where τ_0 is the fluorescence lifetime in the absence of transfer (3.5 ns for R18/F5-TPB at 0.2 wt%), R_0 is the Förster radius for homo transfer (of the order of 5.5 nm) which can be calculated from the spectral data (SI Table S4), and C is the concentration in molecules per nm^3. This yields theoretical values for the anisotropy decay times of the order of 300 ps for 1 wt% and 15 ps for 5 wt% dye loading (see Supporting Information for calculations and values of R_0 and τ_a). Comparison of these theoretical values with the experimental decay times shows good agreement for PCL NPs (300 ps and ~20 ps at 1 and 5 wt%, respectively) and reasonable agreement for

PMMA (180 ps and ~20 ps). However, in the case of PLGA the experimental decay time for 1 wt% is with less than 20 ps far below the theoretical estimation. The obtained decay time of < 20 ps for this case would correspond to an at least five-times higher fluorophore concentration, and suggests again smaller inter-fluorophore distances in the case of PLGA than what would be expected for a random distribution. In contrast, the good agreement between theory and experiment suggests a nearly random (homogeneous) distribution of the fluorophores in the PCL NPs and an only slightly disturbed distribution in PMMA NPs at least up to 5 wt% loading.

Small Angle X-Ray Scattering on Loaded NPs

In order to further address organization of dyes in these NPs we performed small angle X-ray scattering (SAXS) experiments on PLGA and PMMA NPs, either blank or loaded with 5 wt% of R18/F5-TPB, in solution. In Figure 5 the results are shown using the Porod's representation of the NPs' form factors (V_P*P(q); V_P being the volume of the particles and P(q), their form factor such as P(0)=1), that is as I(q)/Q * q^{-4} as a function of q, where I(q) is the scattered intensity, Q the Porod's invariant and q the scattering vector (cf. SI). All curves show a first maximum at scattering vectors around 0.016 $Å^{-1}$, followed by a first minimum and typically a second, less pronounced maximum around 0.037 $Å^{-1}$. The general shape of the curves corresponds well to the form factor of spherical particles, with the first maximum corresponding to the curvature correction to the Porods' law and the plateau to the existence of a sharp interface between particle and solution at low spatial resolution ($2\pi/q_{max}=2\pi/0.06 \approx 100$ Å). The positions of the maxima and the minimum allowed calculating the size of the particles (legend in Figure 5, Supporting Information Table S5). The resulting diameters were quite close to those measured by TEM, and no significant difference between bare and dye-loaded NPs was observed. As

SAXS measurements were performed in aqueous solution, while in the case of TEM the measurements were conducted under high vacuum, and thus in the dry state, these small differences indicate that the particles are only slightly hydrated. It furthermore means that the loading with the fluorophore/counterion pair did not lead to an increase in the hydration. The nanoparticles thus appeared as rather pure polymer "balls" in which the dye was then embedded.

In the case of PMMA NPs the curves of the bare and the dye-loaded NPs were practically superimposed up to the second maximum (beyond which the signal became noisy due to the low contrast of PMMA with respect to water). There was thus no visible effect of the presence of the dye on the internal structure of the particles, which would be in agreement with a relatively homogeneous distribution of the dye within the matrix. In the case of PLGA NPs, on the other hand, clear changes in the scattering curves upon dye loading were observed. In particular, the intensity of the first maximum decreased, while the first minimum is less pronounced, indicating changes in the overall structure of the particles. These changes could stem from the internal organization of the particles, e.g. a non-homogeneous distribution of the dye within the particle, with a higher concentration at the core and very low concentrations close to the surface. Though the precise distribution of the dyes within the particles could not be inferred from this data, comparison of the curves showed that the presence of the fluorophore/counterion pair influences the final structure in the case of PLGA, while practically no changes were observed for PMMA.

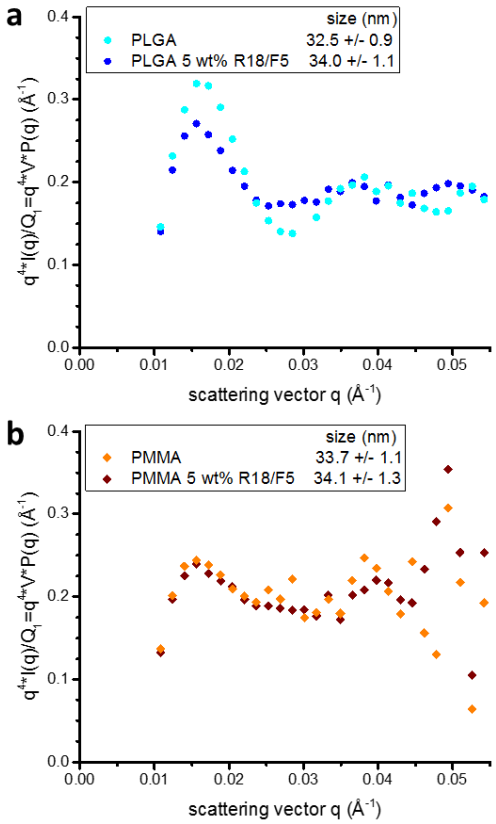

Figure 5. Small angle X-ray scattering of NP solutions. Porod's representation of the NP form factors [V_P*P(q)] for (a) PLGA and (b) PMMA NPs bare and loaded with 5 wt% R18/F5-TPB. Q_I is the Porod's invariant. The diameters of the particles as derived from SAXS measurements are given. Errors correspond to the standard deviation over the results obtained from the different maxima/minima.

NPs Loaded with Perylene Diimide

We then wanted to know whether the described phenomenon of polymer directed organization of the load is unique for the studied dye/counterion system or is an inherent property of the polymer NPs studied. We hence used an uncharged dye from the perylene diimide family, N,N′-Bis(1-heptyloctyl)-3,4,9,10-perylenebis-(dicarboximide) (PDI-1, Figure 1), known to undergo characteristic spectral shifts upon aggregation (Figure 6).[24,52] An increase in loading of PDI-1 into PLGA NPs resulted in the deviation of the absorption spectra relative to that of PDI-1 in dioxane (SI Figure S7), as reported previously.[24] In particular the height of the short-wavelength peak at 490 nm increased relative to the longer-wavelength maximum at 530 nm (Figure 6 c). At the same time the fluorescence spectra showed the appearance of a broad, red-shifted band at ~ 650 nm that increased strongly with dye loading (Figure 6 a, d). Similar variations of absorbance and emission spectra have been reported for aggregates formed by other PDI dyes and naphthalene diimides with similar structure, where the new long-wavelength emission band was assigned to the excimer.[53,54] For the same dye loadings in PMMA-based NPs, these spectral variations were much less pronounced (Figure 6, SI Figure S7), whereas the smallest spectroscopic changes were observed for PCL NPs. Moreover, the QYs of PDI-1 in PMMA and PCL NPs decreased less than in PLGA NPs (Figure 6 b). Together these results indicate that the aggregation state of PDI-1 inside NPs depends on the matrix polymer, with dye aggregation increasing in the following order PCL < PMMA << PLGA. The observed aggregation behavior of PDI-1 as a function of the polymer matrix is similar to that observed for the rhodamine ion pair R18/F5-TPB. This means in turn that the control of dye aggregation through the nature of the polymer is a more general phenomenon, which could be observed for different cargo molecules.

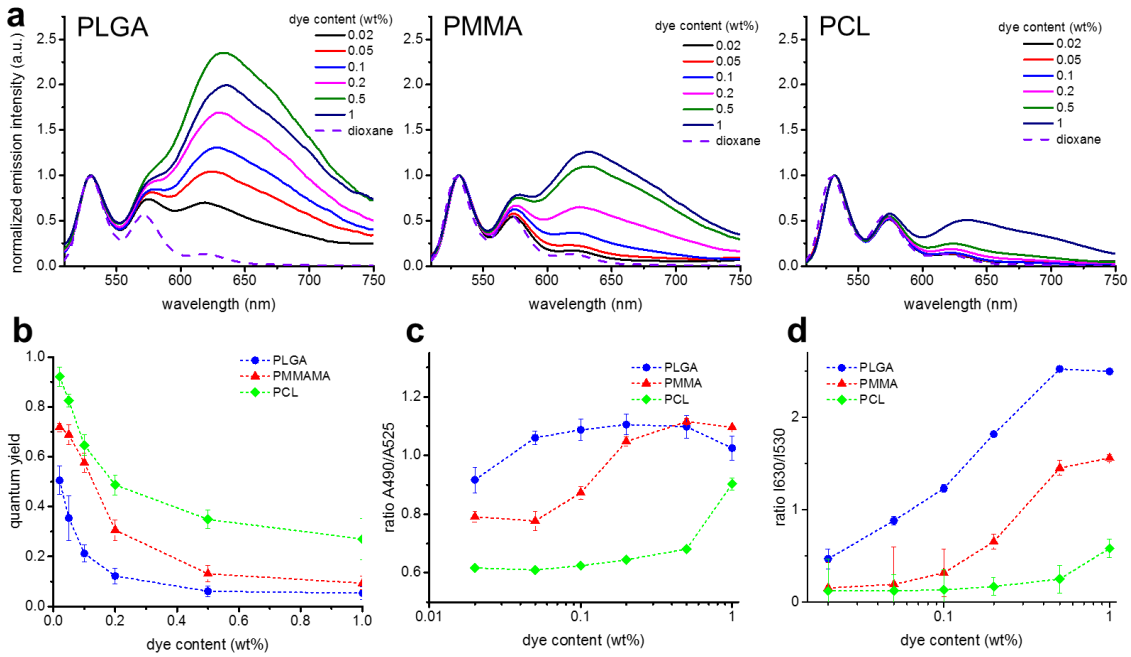

Figure 6. Absorption and emission properties of PDI-1 loaded NPs made from different polymers: (a) Normalized fluorescence emission spectra of NPs of different polymers containing different amounts of PDI-1 and comparison to PDI-1 in dioxane. (Normalization has been performed relative to the peak at 530 nm.) (b) Quantum yields of nanoparticles made from different polymers and loaded with different amounts of PDI-1. QYs were determined relative to rhodamine 101 as standard (QY = 0.9) using an excitation at 530 nm. Given values are averages over at least 3 measurements, error bars correspond to s.e.m. (c) Ratio of absorbance of these NPs at 490 nm and 525 nm. (d) Ratio of fluorescence emission of these NPs at 630 nm and 530 nm.

Solubility of Polymers and Nanoprecipitation

Formation of NPs through nanoprecipitation is a kinetically controlled process.[55,56] We supposed, hence, that differences in the speed of NP formation by the three polymers could be at the origin of the observed differences in organization of the encapsulated compounds in the NPs. One important parameter in the kinetics of particle formation is the supersaturation of the polymer in the acetonitrile water mixture that forms upon addition of the acetonitrile solution to the aqueous phase.[57,58] Both nucleation and growth speed increase with increasing supersaturation. This supersaturation should in turn depend on the solubility of the polymers in mixtures of acetonitrile and water. In order to evaluate these we performed turbidity studies of the polymers by adding increasing amounts of water to solutions of the polymers in acetonitrile (Figure 7 a). Interestingly, turbidity for PCL appeared at the lowest water fraction, followed by PMMA, and finally PLGA. This indicates that, in such mixtures, the solubility of these polymers increases in the order PCL < PMMA < PLGA, in good agreement with decreasing hydrophobicity of these polymers (logP values: 4 for PCL, 2.8 for PMMA, and -0.5 for PLGA[59]). This in turn suggests that, during the fast mixing process, supersaturation should be highest for PCL, leading to the highest particle formation speed.

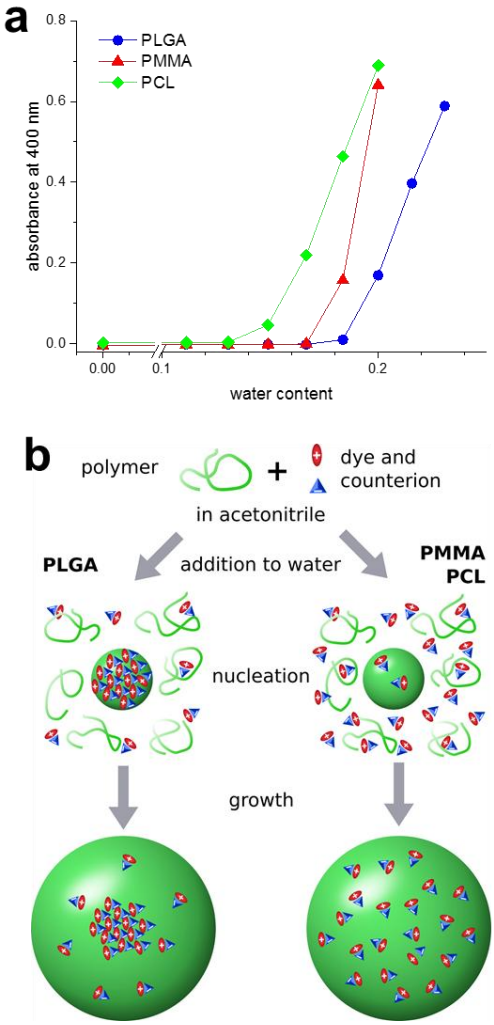

Figure 7. (a) Turbidity measurement of different polymers in acetonitrile water mixtures. Given are the absorbance values measured at 400 nm for polymer solutions in acetonitrile with different water contents. (b) Schematic view of proposed particle formation and dye organization for systems composed of PLGA (left) and PMMA or PCL (right).

Discussion

We found that the optical properties of dyes encapsulated at various concentrations in polymer nanoparticles depend on the type of polymer used as matrix material. Indeed, in PLGA NPs, the dyes showed much faster communication and/or stronger aggregation compared to PMMA and PCL NPs. These results suggest that in the case of PLGA the dyes are inhomogeneously distributed inside the matrix forming clusters of high effective concentration (Figure 7b). This is probably not the case for PMMA and especially PCL, where dyes seem to distribute homogeneously within the particle (Figure 7b).

Such differences in the organization of the load inside the polymer NPs are supposed to be linked to differences in kinetics of their nanoprecipitation, which in turn depend on the hydrophobicity of the polymers (Figure 7). In the case of rather hydrophobic PCL and PMMA, which should undergo fast nanoprecipitation, the dye could simply be captured or integrated during particle growth through a diffusion limited process, leading to a homogeneous distribution of the load within the particle. In the case of the much less hydrophobic PLGA, we expect that the particles are formed much more slowly. Therefore, our highly hydrophobic dyes could have the time to embed into the forming polymeric nuclei at the very beginning of the particle growth. These dyes could also form the nuclei themselves or at least participate in their formation and thus initiate particle formation. Both scenarios could explain the formation of NPs having a core with very high concentration of the load compared to the rest of the particle, in good agreement with the higher effective concentrations of the dyes observed in PLGA NPs. This would also be in line with the changes in the scattering curves observed in the SAXS measurements upon dye loading. Earlier work showed that pure clusters of R18 with excess of

the F5-TPB counterion could also be highly emissive,[39] supporting the present model of a core with high dye concentration and a PLGA-rich shell.

The resulting differences in the organization of the load led to differences in the fluorescence properties. In the case of the dye/counterion pair R18/F5-TPB tuning the effective concentration allowed controlling the distance between fluorophores and thus the speed of excitation energy transfer inside the nanoparticle. This, in turn, opened the way to controlling the blinking behavior of the whole particle ranging from complete particle blinking to complete absence of blinking for a given dye loading - and even to partial blinking for certain loadings. Here, one should mention conjugated polymers: their fluorescence behavior depends strongly on their folding and packing.[60]

To get a better idea why some of our particles show practically complete blinking and others not, it is useful to elude what happens to the excitation energy. The observed one-step switching between the on- and the off-state indicates that whole particle blinking requires collective behavior of all the fluorophores in one particle, which means that the excitation energy has to be able to travel over the whole particle. In other words: the energy should be able to diffuse to a single transient dark species corresponding to an energy sink somewhere in the particle thus creating the off-state. Hence, the first condition for blinking to appear is that all the fluorophores in one particle can participate in energy transfer. Indeed, we found here, and in our previous work,[27] that blinking only occurs in systems, where the number of fluorophores involved in energy transfer N, as calculated from the residual anisotropy r_∞ is of the order of the mean number of fluorophores per particle. This was notably the case here for PLGA already at 1 wt% of dye loading as well as for all three polymers at 5 wt% of dye loading. However, while the

PLGA NPs showed practically complete blinking at these loadings, for PMMA and PCL NPs the fluorescence was stable.

Indeed, our data suggest that a second condition for blinking to occur is sufficiently fast excitation energy migration. For instance, at 1 wt% loading the systems undergoing excitation energy transfer on the time scale of 300 ps, PMMA and PCL, do not blink. However, when the process takes place at <20 ps as in PLGA, whole particle blinking was detected. Considering energy transfer among identical fluorophores as the diffusion of excitons, an exciton diffusion coefficient can be determined according to[61]:

$$D = 0.374 \cdot \left(\frac{4 \cdot \pi \cdot C}{3}\right)^{\frac{4}{3}} \frac{R_0^6}{\tau} \qquad (4)$$

where τ corresponds to the radiation lifetime that can be estimated as the fluorescence lifetime, and R_0 is the Förster radius. This in turn allows determining the mean square distance covered by the exciton during a given time t:

$$\langle x^2 \rangle = 6 \cdot D \cdot t \qquad (5)$$

The square root of this distance corresponds to the radius of the sphere over which the exciton diffuses during the time t. It allows us to estimate the time an excitation needs to travel over a distance equal to the particle size by taking $\sqrt{\langle x^2 \rangle}$ as the radius of the NP (18 nm for the largest NPs here). This time should also correspond to the time it takes the excitation to come within reach of all the fluorophores in the NP (and thus also a possible energy sink located somewhere in the particle). At a dye concentration of 1 wt% and random (homogeneous) distribution in a PMMA or PCL matrix, it would take about 3 ns for the exciton to diffuse over the size of a NP (Figure 5 and S8). For these NPs the exciton diffusion time is thus of the order of the fluorescence lifetime. This means in turn that there is a very large chance of the particle to emit a photon before the excitation energy is transferred to a dark species possibly present in the

particle. At 5 wt% loading and homogeneous distribution, as in PMMA and PCL NPs, the estimated time required for the excitation energy to travel over these particles, and thus to come within reach of a transient dark state, is 400 ps. This still leaves a relatively high probability for fluorescence emission to occur with minimal perturbation by dark states. Some blinking of PMMA and PCL NPs is observed starting from about 20 and 30 wt% dye loading. At these concentrations, the time it takes the exciton to diffuse over a distance corresponding to the NP size is of the order of 50 ps, which results in a relatively high probability of quenching through a single transient dark species. It is clear that the blinking in this case will also depend on the particle size, which is exactly what we observed for PMMA-based NPs loaded with 30 wt% of R18/F5-TPB: small (24 nm) NPs showed complete blinking, whereas the majority of large (60 nm) NPs did not exhibit any blinking.

PLGA NPs on the other hand blink already starting from a dye loading of 1 wt%. In this case, our results showed that the effective concentration of the dye is increased, resulting in a local concentration at least 5 times the global concentration. Such a high local concentration would indicate that the fluorophores are concentrated in a region with a diameter of 17.5 nm within the NP. Using Equation (4) and (5) and this diameter we can again estimate the time it would take the excitation energy to migrate over all the dyes in the particle. For this system the time corresponds to 70 ps, which is remarkably close to the times calculated for PMMA and PCL NPs with fluorophore concentrations at which blinking appears.

Hence, we suppose that, the key requirement for whole particle blinking is ultrafast excitation energy transfer that involves all fluorophores within the particle as early as possible within the excited state lifetime. In this case, the ultrafast energy migration ensures transfer of the excitation energy to a transient dark species somewhere in the particle before the emission takes place. If

this occurs fast enough, a single dark species[41] will be able to quench the whole particle, leading to a dark state. The nature of the dark species itself is difficult to identify, especially as it can be present in very low concentrations and for short times. Several mechanisms could explain formation of the dark species. The first is formation of triplet and/or radical states of rhodamine, which were previously reported to be sufficiently long-lived for this type of dye embedded in a polymer matrix.[62] A second possible mechanism is the formation of transient non-emissive dye aggregates that act as the energy sink. By influencing the distances between the fluorophores the polymer matrix can thus control the blinking behavior of the whole particle.

Importantly, the polymer matrix could also control the aggregation state of the dye PDI-1, and in this way the emission color could be tuned from orange to the near-infrared region, in line with our earlier work.[24] Importantly, for both ionic (R18/F5-TPB) and neutral (PDI-1) dyes, the less hydrophobic polymer PLGA favors dye clustering with short inter-fluorophore distances, in contrast to more hydrophobic PMMA and PCL, where the dyes tend to distribute homogenously. Therefore, we expect that by varying polymer structure, it becomes possible to tune the optical properties of nanomaterials as well as to change the organization of the load inside the matrix.

Apart from its direct benefit for the design of ultrabright labels with controlled blinking for fluorescence imaging, the principles described here could also be of importance for the design of other types of materials that require controlling the collective behavior of large ensembles of chromophores. Among these are notably materials intended for photovoltaics and those used for manipulating photons for information storage and transmission.[7,63,64] Furthermore, polymer nanoparticles (NPs) are systems of choice for targeted delivery and controlled release of drugs[65,66] and as carriers for different types of contrast agents.[67,68] These applications require efficient loading of the functional molecules, complexes, or ions, that are the guests or load, and

their controlled release - or its absence.[69] Our findings show the way to approaches to controlling the organization of the load that could go beyond compartmentalized nanoparticles and towards the fine tuning of the release profile of drugs and combinations of drugs.[70,71]

Conclusion

In this paper we studied the influence of the polymer matrix on the fluorescence properties of dye-loaded polymer nanoparticles over a broad range of dye concentrations. We found that the polymer allows fine tuning the emission behavior of the encapsulated dyes and in particular their collective behavior. Using a rhodamine dye and a bulky hydrophobic counterion, fluorescent nanoparticles almost 100 times brighter than quantum dots could be obtained that featured controlled blinking behavior, ranging from complete on-off switching over partial blinking to complete absence of blinking. In the case of a perylene diimide based dye the polymer matrix allowed controlling the emission color from orange to near-infrared. These differences in behavior are due to the organization of the dyes within the matrix, which enables the control of the speed of energy transfer processes as well as of formation of dye aggregates. The hydrophobicity of the polymer seems to play a crucial role in the kinetically controlled nanoprecipitation processes, tailoring the organization of highly hydrophobic dyes from homogeneously distributed (dissolved) to strongly clustered within the polymer matrix.

ASSOCIATED CONTENT

Supporting Information. Transmission electron microscopy images, dynamic light scattering methods and data, fluorescence lifetimes, data on photostability, details of single particle microscopy and determination of brightness, further data on switching, calculations on FRET, SAXS data analysis, spectra of PDI loaded NPs, lifetime anisotropy data. AVI videos of fluorescence microscopy of nanoparticles made of different polymers with 5 and 30 wt% R18/F5-TPB loading.

AUTHOR INFORMATION

Corresponding Author

*Andreas Reisch and Andrey S. Kymchenko: E-mail: reisch@unistra.fr and andrey.klymchenko@unistra.fr, Phone: ++33 36 88 54 266

Author Contributions

A. R. and A. S. K. introduced the concepts and planned the experiments. A. R. and K. T. prepared particles, performed and analyzed most of the experiments. A. S. K. helped with some data analysis and interpretation. A. Ru. Contributed to characterization of particle size and fluorescence. G. F. and M. R. performed and analyzed SAXS experiments. The manuscript was written through contributions of all authors. All authors have given approval to the final version of the manuscript. ‡ These authors have contributed equally to experiments and data analysis.

Funding Sources

This work was supported by the European Research Council ERC Consolidator grant BrightSens 648528 and by the Agence National de Recherche JC/JC grant supertrack ANR-16-CE09-0007.

ACKNOWLEDGMENT

The authors thank C. Ruhlmann for help with electron microscopy, P. Didier for help with fluorescence microscopy, and Ludovic Richert for help with fluorescence lifetime measurements. This work was supported by the European Research Council ERC Consolidator grant BrightSens 648528 and by the Agence National de Recherche JC/JC grant supertrack ANR-16-CE09-0007.

REFERENCES

(1) Alivisatos, A. P. Semiconductor Clusters, Nanocrystals, and Quantum Dots. *Science* **1996**, *271*, 933–937.
(2) Wegner, K. D.; Hildebrandt, N. Quantum Dots: Bright and Versatile in Vitro and in Vivo Fluorescence Imaging Biosensors. *Chem. Soc. Rev.* **2015**, *44*, 4792–4834.
(3) Green, M. A.; Ho-Baillie, A.; Snaith, H. J. The Emergence of Perovskite Solar Cells. *Nat. Photonics* **2014**, *8*, 506–514.
(4) Manser, J. S.; Christians, J. A.; Kamat, P. V. Intriguing Optoelectronic Properties of Metal Halide Perovskites. *Chem. Rev.* **2016**, *116*, 12956–13008.
(5) Haase, M.; Schäfer, H. Upconverting Nanoparticles. *Angew. Chem. Int. Ed.* **2011**, *50*, 5808–5829.
(6) Alonso-Cristobal, P.; Vilela, P.; El-Sagheer, A.; Lopez-Cabarcos, E.; Brown, T.; Muskens, O. L.; Rubio-Retama, J.; Kanaras, A. G. Highly Sensitive DNA Sensor Based on Upconversion Nanoparticles and Graphene Oxide. *ACS Appl. Mater. Interfaces* **2015**, *7*, 12422–12429.
(7) Joannopoulos, J. D.; Villeneuve, P. R.; Fan, S. Photonic Crystals: Putting a New Twist on Light. *Nature* **1997**, *386*, 143–149.
(8) Fenzl, C.; Hirsch, T.; Wolfbeis, O. S. Photonic Crystals for Chemical Sensing and Biosensing. *Angew. Chem. Int. Ed.* **2014**, *53*, 3318–3335.
(9) Peng, H.-S.; Chiu, D. T. Soft Fluorescent Nanomaterials for Biological and Biomedical Imaging. *Chem. Soc. Rev.* **2015**, *44*, 4699–4722.
(10) Peng, H.-Q.; Niu, L.-Y.; Chen, Y.-Z.; Wu, L.-Z.; Tung, C.-H.; Yang, Q.-Z. Biological Applications of Supramolecular Assemblies Designed for Excitation Energy Transfer. *Chem. Rev.* **2015**, *115*, 7502–7542.
(11) Liu, Z.; Yan, H.; Wang, K.; Kuang, T.; Zhang, J.; Gui, L.; An, X.; Chang, W. Crystal Structure of Spinach Major Light-Harvesting Complex at 2.72 Å Resolution. *Nature* **2004**, *428*, 287–292.
(12) Bopp, M. A.; Sytnik, A.; Howard, T. D.; Cogdell, R. J.; Hochstrasser, R. M. The Dynamics of Structural Deformations of Immobilized Single Light-Harvesting Complexes. *Proc. Natl. Acad. Sci.* **1999**, *96*, 11271–11276.
(13) Zeng, Y.; Li, Y.-Y.; Chen, J.; Yang, G.; Li, Y. Dendrimers: A Mimic Natural Light-Harvesting System. *Chem. – Asian J.* **2010**, *5*, 992–1005.

(14) Hofkens, J.; Maus, M.; Gensch, T.; Vosch, T.; Cotlet, M.; Köhn, F.; Herrmann, A.; Müllen, K.; De Schryver, F. Probing Photophysical Processes in Individual Multichromophoric Dendrimers by Single-Molecule Spectroscopy. *J. Am. Chem. Soc.* **2000**, *122*, 9278–9288.
(15) Yang, J.; Yoon, M.-C.; Yoo, H.; Kim, P.; Kim, D. Excitation Energy Transfer in Multiporphyrin Arrays with Cyclic Architectures: Towards Artificial Light-Harvesting Antenna Complexes. *Chem. Soc. Rev.* **2012**, *41*, 4808–4826.
(16) Peng, H.-Q.; Chen, Y.-Z.; Zhao, Y.; Yang, Q.-Z.; Wu, L.-Z.; Tung, C.-H.; Zhang, L.-P.; Tong, Q.-X. Artificial Light-Harvesting System Based on Multifunctional Surface-Cross-Linked Micelles. *Angew. Chem. Int. Ed Engl.* **2012**, *51*, 2088–2092.
(17) Hong, Y.; Lam, J. W. Y.; Tang, B. Z. Aggregation-Induced Emission. *Chem. Soc. Rev.* **2011**, *40*, 5361–5388.
(18) Wang, L.; Li, Q. Stimuli-Directing Self-Organized 3D Liquid-Crystalline Nanostructures: From Materials Design to Photonic Applications. *Adv. Funct. Mater.* **2016**, *26*, 10–28.
(19) Ostroverkhova, O.; Moerner, W. E. Organic Photorefractives: Mechanisms, Materials, and Applications. *Chem. Rev.* **2004**, *104*, 3267–3314.
(20) Li, K.; Liu, B. Polymer-Encapsulated Organic Nanoparticles for Fluorescence and Photoacoustic Imaging. *Chem. Soc. Rev.* **2014**, *43*, 6570–6597.
(21) Reisch, A.; Klymchenko, A. S. Fluorescent Polymer Nanoparticles Based on Dyes: Seeking Brighter Tools for Bioimaging. *Small* **2016**, *12*, 1968–1992.
(22) Deschout, H.; Zanacchi, F. C.; Mlodzianoski, M.; Diaspro, A.; Bewersdorf, J.; Hess, S. T.; Braeckmans, K. Precisely and Accurately Localizing Single Emitters in Fluorescence Microscopy. *Nat. Methods* **2014**, *11*, 253–266.
(23) Würthner, F.; Kaiser, T. E.; Saha-Möller, C. R. J-Aggregates: From Serendipitous Discovery to Supramolecular Engineering of Functional Dye Materials. *Angew. Chem. Int. Ed Engl.* **2011**, *50*, 3376–3410.
(24) Trofymchuk, K.; Reisch, A.; Shulov, I.; Mély, Y.; Klymchenko, A. S. Tuning the Color and Photostability of Perylene Diimides inside Polymer Nanoparticles: Towards Biodegradable Substitutes of Quantum Dots. *Nanoscale* **2014**, *6*, 12934–12942.
(25) Méallet-Renault, R.; Hérault, A.; Vachon, J.-J.; Pansu, R. B.; Amigoni-Gerbier, S.; Larpent, C. Fluorescent Nanoparticles as Selective Cu(II) Sensors. *Photochem. Photobiol. Sci.* **2006**, *5*, 300–310.
(26) Tian, Z.; Shaller, A. D.; Li, A. D. Q. Twisted Perylene Dyes Enable Highly Fluorescent and Photostable Nanoparticles. *Chem. Commun.* **2009**, 180–182.
(27) Reisch, A.; Didier, P.; Richert, L.; Oncul, S.; Arntz, Y.; Mély, Y.; Klymchenko, A. S. Collective Fluorescence Switching of Counterion-Assembled Dyes in Polymer Nanoparticles. *Nat. Commun.* **2014**, *5*.
(28) Reisch, A.; Runser, A.; Arntz, Y.; Mély, Y.; Klymchenko, A. S. Charge-Controlled Nanoprecipitation as a Modular Approach to Ultrasmall Polymer Nanocarriers: Making Bright and Stable Nanoparticles. *ACS Nano* **2015**, *9*, 5104–5116.
(29) Rust, M. J.; Bates, M.; Zhuang, X. Sub-Diffraction-Limit Imaging by Stochastic Optical Reconstruction Microscopy (STORM). *Nat. Methods* **2006**, *3*, 793–796.
(30) Linde, S. van de; Sauer, M. How to Switch a Fluorophore: From Undesired Blinking to Controlled Photoswitching. *Chem. Soc. Rev.* **2014**, *43*, 1076–1087.

(31) Betzig, E.; Patterson, G. H.; Sougrat, R.; Lindwasser, O. W.; Olenych, S.; Bonifacino, J. S.; Davidson, M. W.; Lippincott-Schwartz, J.; Hess, H. F. Imaging Intracellular Fluorescent Proteins at Nanometer Resolution. *Science* **2006**, *313*, 1642–1645.
(32) Nirmal, M.; Dabbousi, B. O.; Bawendi, M. G.; Macklin, J. J.; Trautman, J. K.; Harris, T. D.; Brus, L. E. Fluorescence Intermittency in Single Cadmium Selenide Nanocrystals. *Nature* **1996**, *383*, 802–804.
(33) Mahler, B.; Spinicelli, P.; Buil, S.; Quelin, X.; Hermier, J.-P.; Dubertret, B. Towards Non-Blinking Colloidal Quantum Dots. *Nat. Mater.* **2008**, *7*, 659–664.
(34) Efros, A. L.; Nesbitt, D. J. Origin and Control of Blinking in Quantum Dots. *Nat. Nanotechnol.* **2016**, *11*, 661–671.
(35) Trofymchuk, K.; Reisch, A.; Didier, P.; Fras, F.; Gilliot, P.; Mely, Y.; Klymchenko, A. S. Giant Light-Harvesting Nanoantenna for Single-Molecule Detection in Ambient Light. *Nat. Photonics* **2017**, *11*, 657.
(36) Demmig, S.; Langhals, H. Leichtlösliche, Lichtechte Perylen-Fluoreszenzfarbstoffe. *Chem. Ber.* **1988**, *121*, 225–230.
(37) Würth, C.; Geißler, D.; Behnke, T.; Kaiser, M.; Resch-Genger, U. Critical Review of the Determination of Photoluminescence Quantum Yields of Luminescent Reporters. *Anal. Bioanal. Chem.* **2014**, *407*, 59–78.
(38) Macdonald, R. I. Characteristics of Self-Quenching of the Fluorescence of Lipid-Conjugated Rhodamine in Membranes. *J. Biol. Chem.* **1990**, *265*, 13533–13539.
(39) Shulov, I.; Oncul, S.; Reisch, A.; Arntz, Y.; Collot, M.; Mely, Y.; Klymchenko, A. S. Fluorinated Counterion-Enhanced Emission of Rhodamine Aggregates: Ultrabright Nanoparticles for Bioimaging and Light-Harvesting. *Nanoscale* **2015**, *7*, 18198–18210.
(40) Tian, Y.; Halle, J.; Wojdyr, M.; Sahoo, D.; Scheblykin, I. G. Quantitative Measurement of Fluorescence Brightness of Single Molecules. *Methods Appl. Fluoresc.* **2014**, *2*, 035003.
(41) Tian, Y.; Merdasa, A.; Peter, M.; Abdellah, M.; Zheng, K.; Ponseca, C. S.; Pullerits, T.; Yartsev, A.; Sundström, V.; Scheblykin, I. G. Giant Photoluminescence Blinking of Perovskite Nanocrystals Reveals Single-Trap Control of Luminescence. *Nano Lett.* **2015**, *15*, 1603–1608.
(42) Bardeen, C. J. The Structure and Dynamics of Molecular Excitons. *Annu. Rev. Phys. Chem.* **2014**, *65*, 127–148.
(43) Colby, K. A.; Burdett, J. J.; Frisbee, R. F.; Zhu, L.; Dillon, R. J.; Bardeen, C. J. Electronic Energy Migration on Different Time Scales: Concentration Dependence of the Time-Resolved Anisotropy and Fluorescence Quenching of Lumogen Red in Poly(Methyl Methacrylate). *J. Phys. Chem. A* **2010**, *114*, 3471–3482.
(44) Ghiggino, K. P.; Reek, J. N. H.; Crossley, M. J.; Bosman, A. W.; Schenning, A. P. H. J.; Meijer, E. W. The Dynamics of Electronic Energy Transfer in Novel Multiporphyrin Functionalized Dendrimers: A Time-Resolved Fluorescence Anisotropy Study. *J. Phys. Chem. B* **2000**, *104*, 2596–2606.
(45) Schlosser, M.; Lochbrunner, S. Exciton Migration by Ultrafast Förster Transfer in Highly Doped Matrixes. *J. Phys. Chem. B* **2006**, *110*, 6001–6009.
(46) Fennel, F.; Lochbrunner, S. Long Distance Energy Transfer in a Polymer Matrix Doped with a Perylene Dye. *Phys. Chem. Chem. Phys.* **2011**, *13*, 3527–3533.
(47) Berberan-Santos, M. N.; Canceill, J.; Gratton, E.; Jullien, L.; Lehn, J.-M.; So, P.; Sutin, J.; Valeur, B. Multichromophoric Cyclodextrins. 3. Investigation of Dynamics of Energy Hopping by Frequency-Domain Fluorometry. *J. Phys. Chem.* **1996**, *100*, 15–20.

(48) Agranovich, V. M.; Galanin, M. D. *Electronic Excitation Energy Transfer in Condensed Matter*; North-Holland Publishing Company, 1982.
(49) Berberan-Santos, M. N.; Valeur, B. Fluorescence Depolarization by Electronic Energy Transfer in Donor–acceptor Pairs of like and Unlike Chromophores. *J. Chem. Phys.* **1991**, *95*, 8048–8055.
(50) Johansson, L. B. A. Limiting Fluorescence Anisotropies of Perylene and Xanthene Derivatives. *J. Chem. Soc.-Faraday Trans.* **1990**, *86*, 2103–2107.
(51) Galanin, M. D. Duration of the Excitation State of Molecules and Fluorescence Properties of Solutions. *Tr. FIAN SSSR* **1950**, *5*, 341–386.
(52) Zhang, X.; Chen, Z.; Würthner, F. Morphology Control of Fluorescent Nanoaggregates by Co-Self-Assembly of Wedge- and Dumbbell-Shaped Amphiphilic Perylene Bisimides. *J. Am. Chem. Soc.* **2007**, *129*, 4886–4887.
(53) Görl, D.; Zhang, X.; Würthner, F. Molecular Assemblies of Perylene Bisimide Dyes in Water. *Angew. Chem. Int. Ed.* **2012**, *51*, 6328–6348.
(54) Würthner, F.; Chen, Z.; Dehm, V.; Stepanenko, V. One-Dimensional Luminescent Nanoaggregates of Perylene Bisimides. *Chem. Commun.* **2006**, *0*, 1188–1190.
(55) Horn, D.; Rieger, J. Organic Nanoparticles in the Aqueous Phase—Theory, Experiment, and Use. *Angew. Chem. Int. Ed.* **2001**, *40*, 4330–4361.
(56) Rao, J. P.; Geckeler, K. E. Polymer Nanoparticles: Preparation Techniques and Size-Control Parameters. *Prog. Polym. Sci.* **2011**, *36*, 887–913.
(57) Lince, F.; Marchisio, D. L.; Barresi, A. A. Strategies to Control the Particle Size Distribution of Poly-ε-Caprolactone Nanoparticles for Pharmaceutical Applications. *J. Colloid Interface Sci.* **2008**, *322*, 505–515.
(58) D'Addio, S. M.; Prud'homme, R. K. Controlling Drug Nanoparticle Formation by Rapid Precipitation. *Adv. Drug Deliv. Rev.* **2011**, *63*, 417–426.
(59) Magenau, A. J. D.; Richards, J. A.; Pasquinelli, M. A.; Savin, D. A.; Mathers, R. T. Systematic Insights from Medicinal Chemistry To Discern the Nature of Polymer Hydrophobicity. *Macromolecules* **2015**, *48*, 7230–7236.
(60) Huser, T.; Yan, M.; Rothberg, L. J. Single Chain Spectroscopy of Conformational Dependence of Conjugated Polymer Photophysics. *Proc. Natl. Acad. Sci.* **2000**, *97*, 11187–11191.
(61) Gochanour, C. R.; Fayer, M. D. Electronic Excited-State Transport in Random Systems. Time-Resolved Fluorescence Depolarization Measurements. *J. Phys. Chem.* **1981**, *85*, 1989–1994.
(62) Zondervan, R.; Kulzer, F.; Orlinskii, S. B.; Orrit, M. Photoblinking of Rhodamine 6G in Poly(Vinyl Alcohol): Radical Dark State Formed through the Triplet. *J. Phys. Chem. A* **2003**, *107*, 6770–6776.
(63) Jr, C. S. P.; Tian, Y.; Sundström, V.; Scheblykin, I. G. Excited State and Charge-Carrier Dynamics in Perovskite Solar Cell Materials. *Nanotechnology* **2016**, *27*, 082001.
(64) Banal, J. L.; Soleimaninejad, H.; Jradi, F. M.; Liu, M.; White, J. M.; Blakers, A. W.; Cooper, M. W.; Jones, D. J.; Ghiggino, K. P.; Marder, S. R.; Smith, T. A.; Wong, W. W. H. Energy Migration in Organic Solar Concentrators with a Molecularly Insulated Perylene Diimide. *J. Phys. Chem. C* **2016**, *120*, 12952–12958.
(65) Bertrand, N.; Wu, J.; Xu, X.; Kamaly, N.; Farokhzad, O. C. Cancer Nanotechnology: The Impact of Passive and Active Targeting in the Era of Modern Cancer Biology. *Adv. Drug Deliv. Rev.* **2014**, *66*, 2–25.

(66) Karimi, M.; Sahandi Zangabad, P.; Ghasemi, A.; Amiri, M.; Bahrami, M.; Malekzad, H.; Ghahramanzadeh Asl, H.; Mahdieh, Z.; Bozorgomid, M.; Ghasemi, A.; Rahmani Taji Boyuk, M. R.; Hamblin, M. R. Temperature-Responsive Smart Nanocarriers for Delivery Of Therapeutic Agents: Applications and Recent Advances. *ACS Appl. Mater. Interfaces* **2016**, *8*, 21107–21133.
(67) Lusic, H.; Grinstaff, M. W. X-Ray-Computed Tomography Contrast Agents. *Chem. Rev.* **2013**, *113*, 1641–1666.
(68) Chen, H.; Ren, X.; Paholak, H. J.; Burnett, J.; Ni, F.; Fang, X.; Sun, D. Facile Fabrication of Near-Infrared-Resonant and Magnetic Resonance Imaging-Capable Nanomediators for Photothermal Therapy. *ACS Appl. Mater. Interfaces* **2015**, *7*, 12814–12823.
(69) Kowalczuk, A.; Trzcinska, R.; Trzebicka, B.; Müller, A. H. E.; Dworak, A.; Tsvetanov, C. B. Loading of Polymer Nanocarriers: Factors, Mechanisms and Applications. *Prog. Polym. Sci.* **2014**, *39*, 43–86.
(70) van Vlerken, L. E.; Duan, Z.; Little, S. R.; Seiden, M. V.; Amiji, M. M. Biodistribution and Pharmacokinetic Analysis of Paclitaxel and Ceramide Administered in Multifunctional Polymer-Blend Nanoparticles in Drug Resistant Breast Cancer Model. *Mol. Pharm.* **2008**, *5*, 516–526.
(71) Linton, S. S.; Sherwood, S. G.; Drews, K. C.; Kester, M. Targeting Cancer Cells in the Tumor Microenvironment: Opportunities and Challenges in Combinatorial Nanomedicine. *Wiley Interdiscip. Rev. Nanomed. Nanobiotechnol.* **2016**, *8*, 208–222.